



LJMU Research Online

Abbas, A, Ruddock, F, Alkhaddar, R, Rothwell, G and Andoh, R

Improving the geometry of manholes designed for separate sewer systems

<http://researchonline.ljmu.ac.uk/id/eprint/10057/>

Article

Citation (please note it is advisable to refer to the publisher's version if you intend to cite from this work)

**Abbas, A, Ruddock, F, Alkhaddar, R, Rothwell, G and Andoh, R (2018)
Improving the geometry of manholes designed for separate sewer systems.
Canadian Journal of Civil Engineering, 46 (1). pp. 13-25. ISSN 0315-1468**

LJMU has developed **LJMU Research Online** for users to access the research output of the University more effectively. Copyright © and Moral Rights for the papers on this site are retained by the individual authors and/or other copyright owners. Users may download and/or print one copy of any article(s) in LJMU Research Online to facilitate their private study or for non-commercial research. You may not engage in further distribution of the material or use it for any profit-making activities or any commercial gain.

The version presented here may differ from the published version or from the version of the record. Please see the repository URL above for details on accessing the published version and note that access may require a subscription.

For more information please contact researchonline@ljmu.ac.uk

<http://researchonline.ljmu.ac.uk/>

Improving the Geometry of Manholes Designed for Separate Sewer Systems

Alaa Abbas¹, Felicite Ruddock², Rafid Alkhaddar³, Glynn Rothwell⁴ and Robert Andoh⁵

¹ Postgraduate Research Student, Liverpool John Moores University, Department of Civil Engineering, Henry Cotton Building, 15-21 Webster Street, Liverpool, L3 2ET, UK, A.H.Abbas@2015.ljmu.ac.uk

² Programme Leader, Department of Civil Engineering, Liverpool John Moores University, Peter Jost Center, Byrom Street, Liverpool L3 3AF, UK, F.M.Ruddock@ljmu.ac.uk

³ Professor of Water and Environmental Engineering and Head of the Department of Civil Engineering, Liverpool John Moores University, The Peter Jost Center, Byrom Street, Liverpool, L3 3AF, UK, R.M.Alkhaddar@ljmu.ac.uk

⁴ Department of Maritime and Mechanical Engineering, Liverpool John Moores University, Byrom Street, Liverpool, L3 3AF, UK, G.Rothwell@ljmu.ac.uk

⁵ Professor Robert Andoh, CEO and President of AWD Consult Inc. 32 Vista Drive, South Portland, ME 04106, USA, bandoh@awdconsult.com

Abstract

The design of manholes dates back more than 100 years. However, there have been developments such as the use of new materials for the manufacture of manholes, and advances in inspection and maintenance technologies, allowing improvements to the shape of manholes. This paper presents an innovative design for manholes, created to overcome the challenges associated with the installation of separate sewer systems in narrow streets, common to both UK and EU cities. The traditional separate sewer system has two separate manholes. The proposed manhole combines these two manholes into one structure, with two separate chambers, to allow storm flow and foul flow to pass through the same manhole without mixing. The structural performance of the new design has been tested using mathematical modelling validated by experimental tests. The results are compared with the structural performance of traditional manholes. The new design shows an improved resistance to high live loads.

Keywords: Innovative design, manhole, mathematical model, separate sewer system, structural performance.

32 **1. Introduction**

33

34 The manhole is one of the main elements of a sewer network, used to gain access to the sewer for
35 inspection and maintenance. The construction of manholes has improved, over time, with reference to
36 the materials used. Originally built of brick, significant improvements were made by using concrete
37 and precast materials. However, corrosion to concrete caused by H₂S means that the inner surface of
38 manholes need to be coated, or newly developed materials such as fiberglass and polyethylene used
39 instead (Ahn et al. 2009; Hughes 2009; Petroff 1994). A manhole needs to provide sufficient working
40 space and safe entry and egress for personnel to the sewer system network (BSEN476 2011). Recently,
41 because of rapid developments in sewer inspection and maintenance equipment technology, many
42 water authorities have started using inspection manholes, instead of the traditional manhole, which
43 has the same design of a manhole but with smaller dimensions, this manhole suitable for equipment
44 entry rather than personnel access (BSEN752:2008 2013). The maximum space between two
45 manholes and location of the manhole should be adequate to allow easy use of this equipment. This
46 means that design criteria require manholes sited at every change of alignment, or gradient, and
47 wherever there is a change in the size of sewer pipes. They also need to be spaced at reasonable
48 intervals for inspection and maintenance, somewhere between 50 and 100 meters (BSEN752:2008
49 2013). Manholes are either rectangular or circular, but from a review of the literature, it is clear that
50 there is a paucity of research on manhole shape or structural performance (Bettez et al. (2001);
51 Saricimen et al. (2003)), specifically regarding combined manholes. A rectangular combined
52 manhole, one manhole structure with two chambers, one for wastewater the other for rainwater, was
53 patented by Würmseher (2014). Willi (1998) patented a design which was the same size as traditional
54 manholes but can be either rectangular or circular with two stage chambers arranged vertically, storm
55 chamber over sanitary. Work examining the structural performance of traditional manholes was
56 carried out by Sabouni and El Naggar (2011a). They used three manholes, two of diameter 1200 mm
57 (one reinforced, the other not), the third of diameter 1500 mm, both built from precast concrete. They
58 used a large-scale (4.5 m x 4.5 m x 7.62 m) geotechnical cell for testing and followed the Canadian
59 Highway Bridge Design Code as a guide for the application of live loads. They found that the range of

60 displacement of the manholes ranged between 1.3 mm and 5.6 mm for all loading tests. They
61 concluded that the frictional resistance along the manhole structure, mitigated the effect of truck
62 loading. All their manholes withstood the truck loads, even the non-reinforced one. Sabouni and El
63 Naggari (2011b) used these results to validate a 3-dimensional Finite Element model (FE) for circular,
64 precast and concrete manholes. The FE model was used to test a different combination of concrete
65 manholes in native soil conditions, including soil compaction, groundwater level, trench dimensions
66 and method of installation. They found that soil water content (groundwater level) creates more stress
67 effects on manhole bases than any other factor. Al-Saleem and Langdon (2016) presented the results
68 of structural tests of a manhole under a single live load, this was part of work to develop and upgrade
69 standardised design guidelines for precast concrete manholes in New Zealand (CPAA 2016). They
70 concluded that the service life of a manhole is typically 100 years and that the designer needs to be
71 aware that the standard design is for normal application but that the manhole can be modified to meet
72 any special site requirements or project applications. IKT (2012) who estimated the total number of
73 manholes in Germany at ten million, conducted a full-scale comparison laboratory experiment study,
74 using cementitious and polymeric coatings to line manholes to improve their structure, and to treat
75 those which were deteriorating. A substantial study was carried out by Najafi and Sever (2015b), who
76 estimated the number of manholes in the USA to be approximately 20 million. Their study tested the
77 structural capabilities of the manhole when lined with specific materials using structure strength tests,
78 mathematical modelling and evaluated case histories. The procedure involved using a small-scale
79 model to validate an FE model, the results of which were used to upgrade the FE model to full scale.
80 The results from both Germany and the USA, revealed that manhole structural performance was not
81 affected by the type of lining or deterioration of said lining. Bandler (2007) conducted a study to test
82 two types of manhole materials; unreinforced concrete and masonry. Manholes were exposed to
83 axisymmetric pressure to simulate horizontal effective loads, the effect of the coating material
84 assessed in order to improve the structural performance of the manhole. Brown and Brown (2000)
85 studied the structural performance of manholes and the combination of vicinity asphalt surfacing
86 under wheel loadings, finding that surface displacement is a result of subgrade deformation rather
87 than manhole deformation.

88 This paper presents a new design for manholes, gathering the two separate sewer manholes (sanitary
89 manhole and storm manhole) into one manhole structure with two separate chambers, one for sewage
90 flow the other for stormwater flow. This new design provides the advantages of decreases in cost and
91 a reduced footprint compared with traditional separate sewer systems, as it allows two pipes to be
92 positioned in one trench and the construction of separate sewer systems in narrow streets. The
93 structural performance (correlation between manhole shape and soil) of the new manhole when buried
94 in soil, was tested in this research. Two prototypes were used; the new design and a traditional
95 manhole. The experimental results were used to validate a numerical model which upgraded the
96 model to real scale. The integrity of the structural performance of the new design has been tested and
97 compared with the structural performance of traditional manholes under the same conditions.

98

99 **2. Design Loads**

100

101 The manhole structure can be exposed to two types of loads; permanent dead loads such as the weight
102 of the manhole structure, road layers, soil backfill and manhole cover, and live loads such as traffic
103 loads and hydrostatic flow load. The traffic load directly effects the manhole cover as it is normally
104 on same level as the street surface. Table 1 shows the different categories of live loads (ASTM-C890
105 2006; BS 2010). The manhole wall needs to be thick enough to resist the compressive forces caused
106 by vertical loads and/or horizontal loads such as lateral earth pressure or hydrostatic pressure (ACPA
107 2008) . The lateral load pressure can be calculated as:

108

$$p = w_s H K_s + 62.4H$$

109

110 where p = total earth and hydrostatic pressure (pounds per square foot); w_s = effective unit weight of backfill
111 material (pounds per cubic feet); H = depth of manhole (feet) and K_s = the conjugate ratio for the soil.

112

113 ASTM-C890 (2006) uses a pyramid method to calculate the distribution of traffic loading through
114 specific cover depths (H) such as pavement layers and filling soil above the structure of the manhole,
115 Equation 1 is used to calculate this load. The tire footprint for dual wheels is simulated by a
116 rectangular plate ($L=50.8$ cm x $W=25.4$ cm), the pressure on the manhole structure being the pressure
117 at the base of the pyramid. Figures 1 and 2 show the distribution of dead loads and live loads on the
118 manholes. In this research, H is taken as zero to apply the maximum load that the top of the manhole
119 can be exposed to.

120 $P=F/(W+1.75H)\times(L+1.75H)$ (Eq 1)

121

122

123

124

125

Fig. 1. Pyramid method for the distribution of a live load "Reproduced, with permission from [ASTM C890-13] copyright ASTM International, 100 Barr Harbor Drive, West Conshohocken, PA 19428."

Fig. 2. cumulative vertical loads "Reproduced, with permission from [ASTM C890-13] copyright ASTM International, 100 Barr Harbor Drive, West Conshohocken, PA 19428."

126

127 **3. Manhole models**

128

129 The conventional, separate sewer system has two manholes; one for sewage, the other for stormwater.

130 The geometrical design of these manholes was created more than 100 years ago, Figure 3 illustrating

131 this design and its setup within a traditional separate sewer system (DEFRA 2011). Normally the

132 dimensions of the conventional manhole are between 1 and 1.8 meters diameter at the intermediate

133 network (between the lateral pipes and trunk pipelines), the exact size dependant on the diameter of

134 the inlet-outlet pipe servicing that manhole. The depth of the manhole is dependent on the level of the

135 outlet pipe and can be 1 meter at the beginning of the network, increasing to a depth of 7 meters

136 before using a lift station to raise the hydraulic gradient again to 1 meter. Novel approaches,

137 techniques and devices mean that the original design criteria established a century ago, is obsolete.

138 The negative impact of the combined sewer system on the environment has necessitated new

139 environmental regulations to encourage the use of separate sewer systems (Bizier 2007). Work is

140 required to comply with new regulations for the protection of the environment, even in areas where

141 the installation of traditional separate sewer systems is challenging (EPA 2007).

142

143

144

145

Fig. 3. Typical design of a sanitary manhole and storm manhole located in a separate sewer system

146

147 This research constitutes a new approach to manhole design by combining the two manholes in a
148 separate system, into a one-manhole structure still keeping both storm flow and sewage flow separate.
149 The new structure has two chambers; an external chamber for stormwater flow and an inner chamber
150 for sewage flow. Figure 4 details the design of the new manhole, Figure 5 detailing a cross section of
151 the new manhole in the street. The first chamber, the outer chamber, has a stormwater inlet and a
152 separate stormwater outlet. The second chamber comprises a sewage inlet and separate sewage outlet.
153 The two chambers are arranged coaxially, the storm pipe set above the sanitary pipe in one trench.
154 The dimensions of the outer chamber are between 2.5 to 3 meters diameter, the depth relative to the
155 level of the storm pipes (both inlet and outlet). The dimensions of the inner chamber range from 0.8 to
156 1.2 meters, the depth dependant on the level of the sanitary pipes (inlet and outlet).
157 The manhole itself can be concrete or plastic e.g. HDPE, PVC or GRP, the same material available for
158 traditional manhole manufacture. Because of this, there should be no difference in the lifetime service
159 of the new manhole in comparison to a traditional manhole. The hydraulic performance of the new
160 manhole however, has a different impact on the serviceability of the sewer system, this requiring more
161 research to establish the hydraulic integrity of the new design. A non-reinforced concrete manhole
162 was used to simulate a real scale model in this research.

163
164

Fig. 4. Innovative design of a manhole for separate sewer systems.

165
166

Fig. 5. Cross section of new manhole located in a separate sewer system.

167
168
169
170

171 4. **Methodology**

172

173 A two-stage approach was followed in this research. In the first stage, the finite element model for
174 the case study was built with all the input criteria determined using lab tests to identify the properties
175 of the materials. Prototypes and experimental work were used to identify the boundary conditions
176 necessary to validate the results from the mathematical model (Brinkgreve 2013). The second stage
177 used the mathematical model to ascertain the real scale dimensions of both manholes; the traditional
178 manhole and new design manhole. The FEA used ABAQUS to test the manhole-soil correlation and
179 identify degree of displacement under four loading categories; medium (HS15), heavy (HS20 and
180 HS25) and one overload (double heavy traffic load) when two trucks pass over the manhole at the
181 same time.

182

183 4.1 *Experimental Work*

184 Two prototypes, one of a traditional manhole with a diameter of 10 cm and depth of 30 cm, the other
185 of the new design with the same dimensions for the inner chamber but with a diameter of 25 cm and
186 depth of 25 cm for the external chamber, were constructed. The manholes were buried in soil in a
187 trench of dimensions 2.5 x 0.5 x 1 meters. The trench was located in a hydraulic rig which was used to
188 apply live loads. The cell load and Linear Variable Differential Transducers (LVDTs), were used to
189 monitor applied loads and displacement of the manhole structure, the data recorded by an MC3
190 recorder. The results were used to validate the FE model, this validation allowing an upgrade to a real
191 scale FE model. Figure 6 illustrates the setup of the trench in the rig, the buried manholes, the location
192 of the load cell and the three (LVDTs) for the new manhole. Figure 7 shows the same set up for the
193 traditional manhole. An important input parameter for the FE model concerns the properties of the
194 materials used. Because this research focuses on the performance of the geometry of the manhole
195 buried in soil and not the stress of the manhole structure, the soil properties have been identified
196 through a series of geotechnical laboratory tests. These identified the degree of elastoplastic
197 behaviour of the soil and the contact relationship between the external surface of the manhole and
198 surrounding soil. A natural top-soil was used, normally available from the first layer of the ground

199 surface around the UK, as this is the zone where manholes are buried. As steel was used to build the
 200 prototype manholes, the friction factor between the steel surface and the soil was also determined.

201
 202
 203
 204
 205

a a
 b b

Fig. 6. Setup of the trench in the rig and location of measurement instruments on the new manhole surface at three points on the edge. **Fig. 7.** Setup of the trench in the rig and location of measurement instruments on the traditional manhole surface at three points on the edge.

206
 207

208 4.2 *Mathematical model*

209 A wide range of tools are available to carry out finite element analyses (FEA), including commercial
 210 packages such as ABAQUS (used in this research), designed for use with complicated geotechnical
 211 issues (Torben Pichler 2012). The development of mathematical tools and improvements to the
 212 library of material applicable for FEA, allows geotechnical engineers to select which tools to use to
 213 successfully solve geotechnical structural problems and simulate structural behaviours when
 214 manholes are embedded in soil. That said, engineers still need to have both a geotechnical background
 215 and a good understanding of the principles of FEA to avoid misjudgements. Soil is a complex media
 216 because the texture of soil includes solid particles and voids, which can be full of air or water, making
 217 predicting and simulating soil behaviour a considerable challenge (Mar 2002). Two FE models have
 218 been created for the prototype simulation in the current research; one to simulate the new manhole,
 219 the other a traditional manhole. The same experimental conditions, dimensions, boundary conditions
 220 and materials were used. Restrictions at the base prevented movement but allowed displacement in
 221 the y-axis for the external model's faces and used the symmetry around the x-axis and z-axis for the
 222 internal faces to simulate the full model behaviour. The symmetry of the model around the x-axis and
 223 z-axis allows the use of a quarter model using the specific tools in Abaqus. The creation of a

224 symmetrical model and use of only one quarter of the model decreases the run time while giving the
225 same results as a full 3D model . Surface to surface contact interaction was fixed with a friction factor
226 0.45 between the soil and steel, this determined from the experimental test. Figure 8 shows the mesh
227 for the symmetrical quarter of the new manhole model which has 45370 nodes, 35350 elements,
228 35269 linear hexahedral elements of type C3D8R and 81 linear wedge elements of type C3D6. Figure
229 9 shows the mesh for the symmetrical quarter of the model of the traditional manhole which has
230 40532 nodes, 34928 elements, 34856 linear hexahedral elements of type C3D8R and 72 linear wedge
231 elements of type C3D6.
232
233

Fig. 8. The symmetrical quarter of the new manhole FE mesh model representing the full 3D manhole.

Fig. 9. The symmetrical quarter of the traditional manhole FE mesh model representing the full 3D manhole.

234
235
236
237

238 **5. Results and discussion**

239
240
241

240 *5.1 Prototype experimental results*

242

242 Loads have been applied to verify the capacity of the new manhole compared to the traditional
243 manhole, and to calculate the manhole shape – soil correlation. Four categories of loads were
244 simulated; medium traffic HS15, heavy traffic HS20 and HS25 and overload (double heavy traffic).
245 Figure 10 details the response of the new manhole under static applied loads, HS15, HS20, HS25, a
246 double HS25 and a dynamic double HS25, applied load at the end of the test, to establish the
247 maximum resistance. The displacement experienced by the new manhole was within acceptable
248 limits, the standard requirement being 13 mm (Sabouni and El Naggar 2011a), when under HS15,
249 HS20 and HS25 loadings. Displacement was 3.3 mm at HS15, 6.2 mm at HS20 and 9.2 mm at HS25.
250 When the applied load was increased to over load (twice the heavy load HS25), the new manhole
251 continued to be stable but the displacement was 22 mm, which is above acceptable limits. Soil density
252 and the degree of compaction of the filling soil, play a significant role in the stability of buried

253 manholes under live loads (Abolmaali and Kararam 2010). Therefore, the same set of tests were
254 applied to the traditional manhole, the results presented in Figure 10. Displacements were 2.9 mm for
255 a load of HS15, 7 mm for HS20, 14.3 mm for HS25, the manhole sinking into the soil when HS25
256 was doubled. Steel was used to build the manhole prototype because of difficulties fabricating small
257 prototypes of concrete. The friction factor between the steel and soil is less than the friction factor
258 between concrete and soil meaning that the degree of displacement will be lower when concrete is
259 used because the friction factor will be higher.

260
261 The comparisons between the displacement of the new manhole with the traditional manhole in
262 Figure 10, show that under a medium load (HS15), the traditional manhole has less displacement
263 compared to the new manhole. This is because the new manhole is heavier than the traditional one,
264 this adding a significant dead load. However, the effect of manhole weight is smaller when the traffic
265 load is increased. Against the application of heavy loads, the geometry of the manhole plays an
266 important role, improving the resistance of the manhole.

267
268

Fig. 10. Comparison between the new and traditional manholes under the same conditions and live loads.

269
270

271 5.2 *The results from the mathematical model.*

272

273 The same series of loads (HS15, HS20 and HS25) and the exact boundary conditions as for the
274 physical model, were applied on manholes using a finite element model. Selecting the proper
275 constitutive model (stress–strain relationship) to simulate soil behaviour is an important aspect to
276 consider when using FE for soil models (Lees 2012). In this research, two constitutive models
277 (Mohr-Coulomb and Drucker-Prager) have been tested to identify the most appropriate model (Abbas
278 et al. 2017). The properties of the soil were defined by conducting three conventional triaxial
279 compression tests and one isotropic consolidation (compression) test, to establish the elastoplastic
280 behaviour of the soil (Helwany 2007). Table 2 lists the parameters for the materials. A point at the
281 center of manhole was selected to record displacement results because the maximum displacement

282 occurs at the center. Figure 11 shows the results when a double heavy load was applied. The results
283 for each applied load shows the displacements at the same point, these compared with the results of
284 the measurements taken at the cover of the manhole for the experimental tests, under the same series
285 of loads.

286
287

Fig. 11. The displacement of the new manhole at a double heavy load shown in a 3D quarter symmetric FEA model.

288

289 The FE model output and the experiment model have a very close match regarding the displacement
290 of the new manhole under live loads, as demonstrated in Figure 12.

291

292

Fig. 12. Comparison of the displacements from both the experimental work and the FE model for the new manhole, in soil, under live loads.

293

294 The same point was selected to show the displacement results for the traditional manhole, a sample of
295 the results at a double heavy load are presented in Figure 13.

296

297

Fig. 13. The displacement of the traditional manhole at a double heavy load shown in a 3D quarter symmetric FEA model.

298

299

300

301 The comparison of the results from the FE model and the experiment model reveal a close match
302 regarding displacement at low loads and between displacements for the traditional manhole under
303 high live loads. The experimental measurements and FEA results gave a reliable assessment of the
304 behaviour of the geometry of the manhole and estimations of the margins of error expected from the
305 FEA. The experimental test and the FE model results for the traditional manhole are presented in
306 Figure 14.

307

308

309

Fig. 14. Comparison of the displacement results from both experimental works and the FE model for the traditional manhole prototype in soil under live loads.

310

311

312 One of the important validation processes is the comparison of the FE model with lab experimental
313 results to eliminate uncertainty and manage discrepancies in the model thus increasing confidence in
314 the real application (Moser and Folkman 2008). Validation makes the designer more aware of the
315 inevitable inaccuracies between a real case study and an FE model (Mar 2002). The two stages
316 explained above, illustrate that all necessary steps to check and validate the accuracy of the FE model
317 have been taken. All the boundary conditions, contact interactions, material properties and steps were
318 identified correctly, meaning it was possible to upgrade the FE model to a real-life scale with
319 confidence.

320

321

322 *5.3 The real FE model results*

323

324 Normally the dimensions of traditional manholes used in most sewer networks are 1 to 1.8 meters
325 diameter, the depth ranging from 1 to approximately 7 meters. Real scale dimensions were selected
326 for intermediate networks in the sewer system where new systems were expected to be located. The
327 traditional manhole was 1.3 meters in diameter and 3.4 metre deep; the storm chamber of the new
328 manhole 2.8 meters in diameter and 2.65 meters deep, the sanitary chamber having the same
329 dimensions as the traditional manhole. The soil was of 8.5 meters radius and 15 meters deep to
330 identify the maximum area affected by force (Brinkgreve 2013). The same soil properties as for the
331 prototype model, were used for the real scale module. Non-reinforced concrete (Najafi and Sever
332 2015b), was used for the manhole material. The new manhole had 143345 nodes and 138100 elements
333 element types (C3D6 & C3D8R). Figure 15 illustrates the setup of the new manhole in soil.
334 Regarding the traditional manhole, the mesh used was finer to control for the instability found during
335 experimental testing and to avoid aborting the test as a result of the substantial displacement that can
336 occur. The number of nodes was 377705, 373240 elements, the element types the same as for the new
337 manhole (C3D6 & C3D8R). Figure 16 illustrates the setup of the traditional manhole model in soil.

Fig. 15. Setup of the real scale of new manhole – soil model. **Fig. 16.** Setup of the real scale of traditional manhole-soil model.

338

339

340

341 The data regarding the FE model were taken at the center point of the manhole base for both the new

342 and traditional manhole. The maximum displacement at the base of the both manholes was identified.

343 The new manhole is stable, even under high loading (loads 360 KN), the displacement of the soil

344 below the manhole centerline being 8.16 mm, 3.55 mm under loading HS25 (90kN), 3.3 mm when the

345 load was HS20 (70-80 kN) and approximately 3 mm when the load was HS15 (50-60kN). These

346 results reflect high stability against very high loads, more than double the loads that normally occur.

347 The displacements for the traditional manhole had less stability under high loads (loads 360 KN)

348 because the area of the base is smaller than that of the new manhole. The displacement of soil below

349 the manhole centerline was 11.8 mm at 360 kN, 3.4 mm when the load was HS25 (90kN), 3 mm when

350 the load was HS20 (70-80 kN) and 2.7 mm when the load was HS15 (50-60kN). The traditional

351 manhole has less displacement under medium loads and about the same displacement under heavy

352 loads compared with the displacement of the new manhole under the same loads. It also experiences

353 higher displacement under over-loads in comparison to the new manhole. The traditional manhole has

354 less displacement under medium (HS15) loads compared to the new manhole, because of the

355 increased weight of the new manhole which, this adding an extra load to the live load causing

356 additional displacement. Figure 17 shows a comparison of the displacement of the soil below the new

357 and traditional manholes.

358

359

360

361

362

Fig. 17. A comparison of the displacement for both manholes under different loads (FE model).

363

364

365 The results for displacement to both manhole covers and the soil surface for the new manhole,
366 indicates that the new manhole has more impact on the surrounding soil as it was displaced between
367 1-2 mm, under medium and heavy loads (50 to 90 kN), affecting a 3-meter circle around the manhole.
368 This displacement increased to between 2-3.5 mm under a double-heavy load. This displacement
369 represents a summation of the soil displacement below the manhole and the deformation of the
370 manhole material. The displacement increases from 8.16 mm to 9.95 mm under extreme loading, from
371 3.55 mm to 4 mm when the load was HS25 (90kN), from 3.3mm to 3.8 mm when the load was HS20
372 (70-80 kN) and from 3 mm to 3.48 mm when the load was HS15 (50-60 kN). These surface
373 displacements need to be taken into consideration when designing road surfaces as the soil
374 displacement below the manhole base affects connecting manhole pipes. This is critical in many cases
375 of sewer collapse, the collapse happens at the connection joint between the pipes and the manhole
376 because of relative displacement. There was less displacement with the new manhole model, both
377 total surface and soil below the manhole. This increases the safety of sewer systems subject to very
378 high loads. The stress results for the new manhole revealed that the maximum stress is on a slab
379 positioned at the external wall of the storm chamber. The stress is decreased in the direction of the
380 center of the manhole and increased slightly in the area close to the internal wall. The displacement
381 occurring in the traditional manhole surface increased from 11.8 mm to 12.3 mm under high loads.
382 This includes the displacement of the soil underneath manhole and the manhole structure deformation,
383 from 3.4 mm to 3.6 mm when the load was HS25 (90kN), from 3 mm to 3.2 mm when the load was
384 HS20 (70-80 kN) and from 2.7 mm to 2.85 mm when the load was HS15 (50-60kN). These results
385 show that the traditional manhole has less displacement under medium loads and about the same
386 displacement as the new manhole design under heavy loads. It has high displacement under over-
387 loads which are close to failure at 13 mm. A smaller manhole has less impact on the surrounding
388 surface soil, displacements between 1-2 mm across all loads. The stress in the surrounding soil
389 generated by the traditional manhole structure was higher than the stress experienced by the new
390 manhole. It was about three times higher, in comparison to the new manhole which has a larger
391 surface area working to mitigate load stress effects. This reduction in stress is promising as it may
392 allow the use of lightweight materials such as GRP, HDPE or PVC to build the whole, or part of, the

393 manhole structure, e.g. the inner chamber, while using concrete for the external chamber (the storm
394 chamber). There is also the potential to decrease the thickness of the walls, or to minimise the amount
395 of reinforced steel required.

396

397

398

399 *5.4 Investigation of manhole body structure*

400

401 The change in geometry of the manhole created a change in its structural behaviour. The non-
402 reinforced traditional manhole has been previously tested by Sabouni and El Nagggar (2011a) who
403 used two manholes of 1200 mm and 1500 mm. They used 52 MPa as the cylinder compressive
404 strength for the concrete of the base manhole, this a relatively high strength. Their results indicated
405 that both manholes were able to withstand the applied loads, the maximum overall calculated strain
406 approximately 75% in the 1200 mm manhole and 83% in 1500 mm manhole less than the base
407 cracking strain. Sabouni and El Nagggar (2011b) also generated a numerical model (FE) for both
408 manholes. They found that the cracking moment (M_{cr}) of the manhole bases was 16.3 kN·m/m for the
409 1200 mm manhole and 62.4 kN·m/m for 1500 mm manhole, the average bending moment calculated
410 at 4.8 kN·m for the 1200 mm manhole and 10.25 kN·m for the 1500 mm manhole. Further to this,
411 Najafi and Sever (2015a) carried out testing and an FE study for a manhole of 1200 mm, reporting the
412 maximum strain as 0.00019 and the maximum moment as 1 kN·m/m compared with a calculated
413 cracking moment of 15.43 kN·m/m. They used non-reinforced concrete, which has a 40 MPa cylinder
414 compressive strength. It should also be noted that they applied a low load (HS15), approximately 53
415 kN, to the manhole.

416 The same procedure and materials as used by Najafi and Sever (2015a) were used in this research.
417 The applied load however was different as we applied conservative traffic loads to the manhole. Table
418 2 shows the properties of the concrete used for the manhole. ACI318 limits the strain in the concrete
419 to 0.003. The cracking moment of the concrete is calculated using an ACI318 equation (3), 22.7 kN-m
420 for the base of the traditional manhole and 34.1 kN-m for the new manhole. These limits were used to

421 compare the output of both structural manhole models. Table (3) illustrates the maximum strain on the
 422 manhole body and the percentage difference for the bending moment of the base manholes compared
 423 with the cracking moment.

424

425 According to ACI318 the cracking moment of the concrete is calculated as follows:

426

$$427 \quad M_{cr} = \frac{f_{cr} I_g}{y_t} \dots\dots\dots(\text{Eq 2})$$

428

429 For circular concrete slabs, it is

430

$$431 \quad M_{cr} = \frac{f_{cr} b h^2}{6} \dots\dots\dots(\text{Eq 3})$$

432

433

434 where I_g is the gross moment of inertia (m^4); b and h are the width and thickness of manhole base
 435 slab, and f_{cr} is the flexural cracking strength.

436

437 Figures 18a and b show the strain and location of the maximum bending moment in the base of the
 438 manhole for both the new manhole body and the traditional manhole body, under a double heavy load
 439 (180kN). The new manhole almost failed under double heavy loads, this the extreme case, while the
 440 traditional manhole was able to withstand this extent of loading. Double heavy loads are used in this
 441 study to test the maximum structural capacity of the manhole. The manhole body structure will be
 442 studied in detail using reinforced concrete and light-weight materials such as GRP or HDPL in a
 443 subsequent study. We will also investigate if the provision of a flexible joint between the sanitary
 444 wall chamber and the base of storm chamber can improve the structural performance of the manhole.
 445 The structure of the new manhole body can effected by the degree of compaction of the soil
 446 underneath the two chambers of the manhole. Any difference in soil stiffness below these chambers
 447 can led to differential settlement which generates more stress in the body of the manhole depending
 448 on the location of the applied load. Therefore, reinforced concrete is required for the new manhole
 449 design when it is not being laid in a narrow street and can be exposed to double heavy loads.

Fig. 18 a. The strains and location of maximum bending moment in the base of the new manhole body under a double heavy load (180kN).

Fig. 18 b. The strains and location of maximum bending moment in the base of the traditional manhole body under a double heavy load (180kN).

450 **6. Conclusions**

451
452 The technological development of inspection and maintenance equipment for sewer systems, in
453 combination with the availability of new materials for pipe and manhole manufacture, has allowed
454 improvements to be made to traditional manholes. Environmental regulations in many developed and
455 developing countries, require separate sewer systems to be built as combined sewer systems are no
456 longer acceptable. As a response, this research has presented a new design for manholes, siting the
457 two traditional separate sewer system manholes together in one manhole structure, improving on the
458 installation method of separate sewer systems in narrow streets. It has two separate chambers; an
459 external chamber used to carry storm flow and an inner chamber used for sewage flow. Because of the
460 design, it is bigger and heavier in comparison to the traditional manhole. Structural performance
461 testing was carried out using 3D finite element analysis and compared to the performance of
462 traditional manholes. The results revealed that:

- 463 • The weight of the new manhole added a dead load to the loads applied, this affecting the
464 behaviour of the manhole. The displacement was higher than that for a traditional manhole under
465 a small live load.
- 466 • Under heavy loads, both the new and traditional manhole exhibit the same behaviour (settlement)
467 and both operate within standard limitations.
- 468 • The new manhole has very good stability under extremely high loads; the traditional manhole
469 experienced more settlement under the same load.
- 470 • The new manhole was stable and had less displacement under a double heavy load. However,
471 the bending moment was close to the cracking moment at the base of the storm chamber under a
472 double heavy load; reinforcement was recommended for the slab (cover) and the base of the
473 manhole. This will be examined in the next stage of the current research.
- 474 • The levels of soil stress in the new manhole were dramatically reduced, in comparison to soil
475 stress in the traditional manhole structure, under identical loads.

476 The structural improvements generated by the mathematical model (successfully calibrated by the
477 experimental work), allow the safe use of this new manhole in narrow streets, prevalent in the UK and

478 EU, which up to now have constituted a real challenge when constructing traditional separate sewer
479 systems. The displacement of the new manhole is higher than the displacement of the traditional
480 manhole, under low loads, because of the weight of the new manhole. This effect is expected to
481 disperse through the construction stage under good compaction processes. The new manhole shows
482 high stability and resistance against high live loads. The stress created by live loads on the new
483 manhole was significantly lower than that for traditional manholes. This implies that a review can be
484 made of the thickness and reinforcement required for the walls of the manhole, including the potential
485 to use lighter materials such as GRP, HDPE and PVC in the manufacture of new structures.

486

487 **Acknowledgements**

488 The first authors would like to express their sincere thanks to the Al Ghalowa Company for their
489 support. Thanks are also extended to LJMU technical staff for providing the necessary support to
490 carry out the experimental testing.

491

492

493 **References:**

- 494 Abbas, A., Ruddock, F., Alkhaddar, R., Rothwell, G., and Andoh, R. 2017. Pipeline–Soil Interaction
495 Simulation under Live Loads Using Elastoplastic Finite Element Models with Laboratory Validation,
496 California, USA ASCE.
- 497 Abolmaali, A., and Kararam, A. 2010. Nonlinear Finite-Element-Based Investigation of the Effect of
498 Bedding Thickness on Buried Concrete Pipe. *Journal of Transportation Engineering* **136**(9): 793-799.
- 499 ACPA, A.C.P.A. 2008. Design data 20: Circular precast concrete manhole. American Concrete Pipe
500 Association, Virginia, USA.
- 501 Ahn, N., Park, D.K., Lee, J., and Lee, M.K. 2009. Structural test of precast polymer concrete. *Journal*
502 *of Applied Polymer Science* **114**(3): 1370-1376.
- 503 Al-Saleem, H.I., and Langdon, W. 2016. Precast Concrete Manholes - A review and Upgrade of
504 Current Practice. *In* WATER NEW ZEALAND 2016 STORMWATER CONFERENCE, NEW
505 ZEALAND.
- 506 ASTM-C890. 2006. Standard Practice for Minimum Structural Design Loading for Monolithic or
507 Sectional Precast Concrete Water and Wastewater Structures. American Section of the International
508 Association for Testing Materials, United States.
- 509 Bandler, A. 2007. The Structural Capacity of Repaired Manholes, Department of Civil Engineering,
510 Queen’s University, Kingston, Canada.
- 511 Bettez, J., Townsend, R.D., and Comeau, A. 2001. Scale model testing and calibration of City of
512 Ottawa sewer weirs. *Canadian Journal of Civil Engineering* **28**(4): 627-639.
- 513 Bizier, P. 2007. Gravity Sanitary Sewer Design and Construction. American Society of Civil
514 Engineers, USA
- 515 Brinkgreve, R.B.J. 2013. Validating Numerical Modelling in Geotechnical Engineering. NAFEMS.
- 516 Brown, S.F., and Brown, C.J. 2000. The structural characteristics of manhole installations in
517 pavements.
- 518 BS. 2010. BS 9295:2010 - Guide to the structural design of buried pipelines. BSI, UK.
- 519 BSEN476. 2011. General requirements for components used in drains and sewers. BSI British
520 Standards, UK. p. 25.
- 521 BSEN752:2008. 2013. Drain and sewer systems outside buildings. British Standards, UK.
- 522 CPAA, C.P.A.o.A. 2016. Loads on Circular Precast Concrete Manholes and Access Chambers. *In*
523 GUIDANCE NOTE (NZ), Australia. p. 8.

- 524 DEFRA. 2011. National Build Standards Design and Construction of new gravity foul sewers and
525 lateral drains. *In* Water Industry Act 1991 Section 106B, Flood and Water Management Act 2010
526 Section 42. Department for Environment Food and Rural Affairs, UK. p. 36.
- 527 EPA, U.S.E.P.A. 2007. Innovation and Research for Water Infrastructure for the 21st Century, USA.
- 528 Helwany, S. 2007. Applied Soil Mechanics with ABAQUS Applications. John Wiley & Sons, Inc.,
529 Hoboken, NJ, USA.
- 530 Hughes, J.B. 2009. Manhole Inspection and Rehabilitation. American Society of Civil Engineers
531 ASCE, Reston, Va.
- 532 IKT, I.f.U.I. 2012. Rehabilitation of Wastewater Manholes: Large Scale Tests and in-Situ Studies
533 Institute for Underground Infrastructure, Germany
- 534 Lees, A. 2012. Obtaining Parameters for Geotechnical Analysis. NAFEMS.
- 535 Mar, A. 2002. How To Undertake Finite Element Based Geotechnical Analysis. NAFEMS.
- 536 Moser, A.P., and Folkman, S. 2008. Buried Pipe Design McGraw-Hill.
- 537 Najafi, M., and Sever, V.F. 2015a. Structural Capabilities of No-Dig Manhole Reha. Water
538 Environment Research Foundation, USA
- 539 Najafi, M., and Sever, V.F. 2015b. Structural Capabilities of No-Dig Manhole Rehabilitation. Water
540 Environment Research Foundation.
- 541 Petroff, L.J. 1994. Design methodology for high density polyethylene manholes. *In* Buried Plastic
542 Pipe Technology. *Edited by* D. Eckstein. ASTM STP 1222. pp. 52–65.
- 543 Sabouni, R., and El Naggar, M.H. 2011a. Circular precast concrete manholes: experimental
544 investigation. *Canadian Journal of Civil Engineering* **38**(3): 319-330.
- 545 Sabouni, R., and El Naggar, M.H. 2011b. Circular precast concrete manholes: numerical modeling.
546 *Canadian Journal of Civil Engineering* **38**(8): 909-920.
- 547 Saricimen, H., Shameem, M., Barry, M.S., Ibrahim, M., and Abbasi, T.A. 2003. Durability of
548 proprietary cementitious materials for use in wastewater transport systems. *Cement and Concrete*
549 *Composites* **25**: 421-427.
- 550 Torben Pichler, T.P., Thorben Hamann, Sascha Henke, Gang Qiu. 2012. High-Performance Abaqus
551 Simulations in Soil Mechanics Reloaded – Chances and Frontiers, USA, May 15-17, Dassault
552 Systèmes
- 553 Willi, G. 1998. Schacht für Kontroll-, Wartungs- oder Reparaturarbeiten *Edited by* E.P. Office,
554 Germany. p. 2.
- 555 Würmseher, H. 2014. Abwasserschacht (Manhole) *Edited by* D.P.-u. Markenamt, Germany p. 7.

Table 1: Vehicle load designations

Designation	Load, max	Uses
ASTM HS25	(89 200 N) per wheel	heavy traffic
ASTM HS20	(71 200 N) per wheel	heavy traffic
ASTM HS15	(53 400 N) per wheel	medium traffic
ASTM H10	(35 600 N) per wheel	light traffic
Extreme heavy load	185 kN	One wheel from 4 th axle (heaviest wheel load) with load factors 2.1 and 2.4 (Sabouni and El Nagggar 2011b)
	207 kN	
	2×112.5 kN	Main roads 112.5 kN wheel loads including an impact factor of 1.3
Loading according to BS 5400 (2:1978) cited in BS 9295:2010	2×105 kN	Light trafficked roads 105 kN wheel loads including an impact factor of 1.5
	2×60 kN	Fields 60 kN wheel loads, including an impact factor of 2.0

Table 2: Model parameters

Items	Parameters	Value		
	Density	1685 kg/m ³		
	E	16.943 MPa		
	ν	0.295		
Soil	Drucker –Prager			
	β	50		
	K	0.8		
	ψ	15		
Steel	Density	7850 kg/m ³		
	E	210GPa		
	ν	0.3		
Bedding	Density	1855 kg/m ³		
	E	100MPa		
	ϕ	35		
	C	0		
	ν	0.4		
Concrete	Density	2200 kg/m ³		
	E	29,992 MPa		
	ν	0.2		
	Plasticity			
	Dilation Angle	38		
	Eccentricity	0.1		
	f_{t0}/f_{c0}	1.16		
	K	0.667		
	Viscosity Parameter	10 ⁻⁷		
	Compressive Behaviour			
	Yield stress	27,000 kPa	39,990 kPa	
	Inelastic Strain	0	0.01	
	Tensile Behaviour			
Yield stress	5000 kPa	2200 kPa	50 kPa	
Cracking strain	0	0.006	0.015	

Table 3. Percentage difference for the bending moment of the manhole bases, the cracking moment and the maximum strain on the body of the manhole.

Load categories	New Manhole design			Traditional manhole design		
	Bending moment	% Diff from the M_{cr}	Max Strain	Bending moment	% Diff from the M_{cr}	Max Strain
HS15	11.9	65%	4.29×10^{-5}	4.27	81%	3.6×10^{-5}
HS20	13.73	60%	4.89×10^{-5}	4.87	78%	4.1×10^{-5}
HS25	15.38	55%	5.5×10^{-5}	5.46	75%	4.5×10^{-5}
Double heavy load	30.23 – 33.54	11% -1.7%	1×10^{-4} – 1.2×10^{-4}	10.68 – 11.815	53% - 48%	8.9×10^{-5} – 9.8×10^{-5}

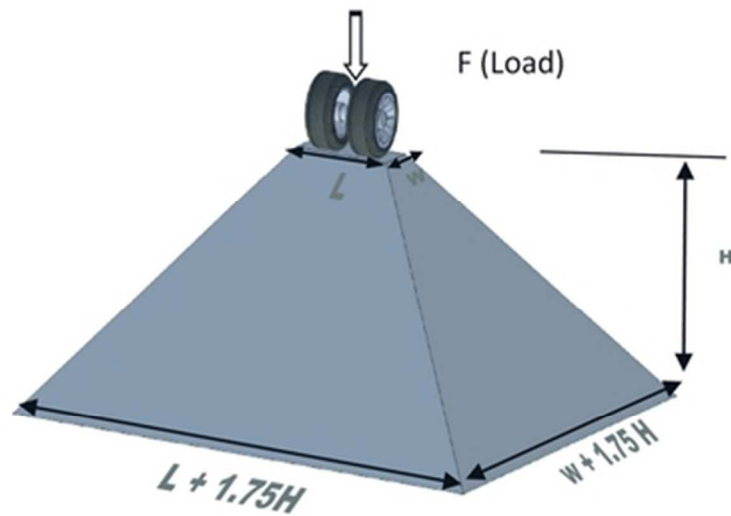


Figure 1. Pyramid method for the distribution of a live load

Fig. 1. Pyramid method for the distribution of a live load "Reproduced, with permission from [ASTM C890-13] ASTM International"

75x54mm (150 x 150 DPI)

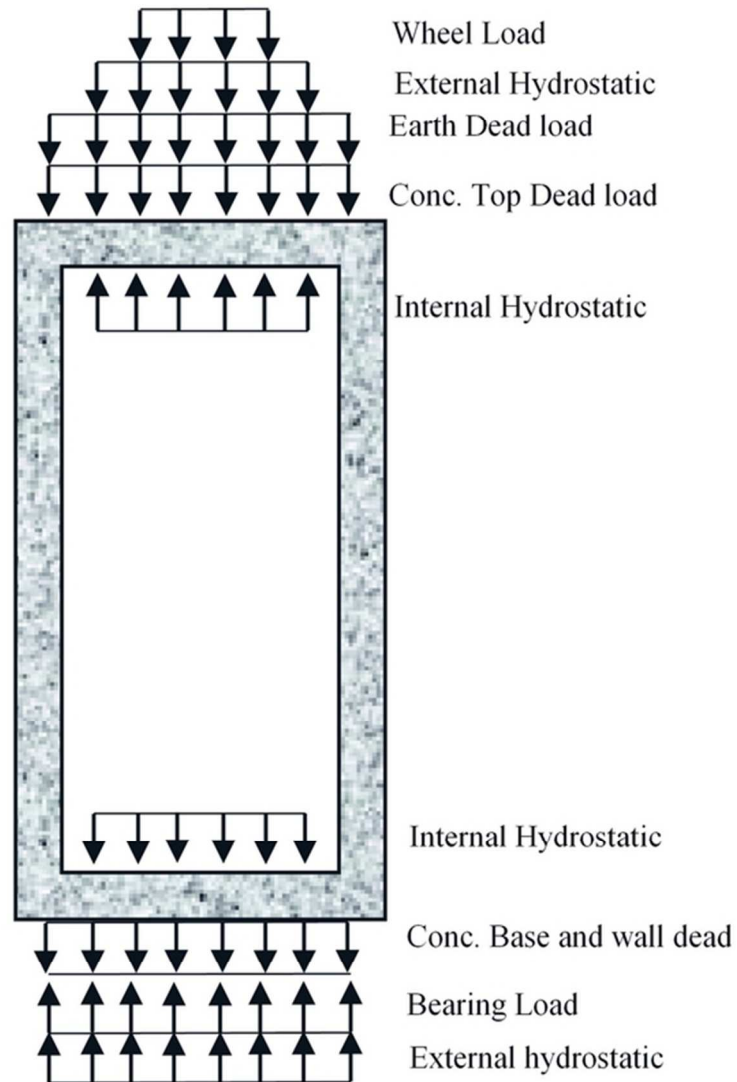


Figure 2. Cumulative vertical loads

Fig. 2. cumulative vertical loads "Reproduced, with permission from [ASTM C890-13] ASTM International"

107x148mm (150 x 150 DPI)

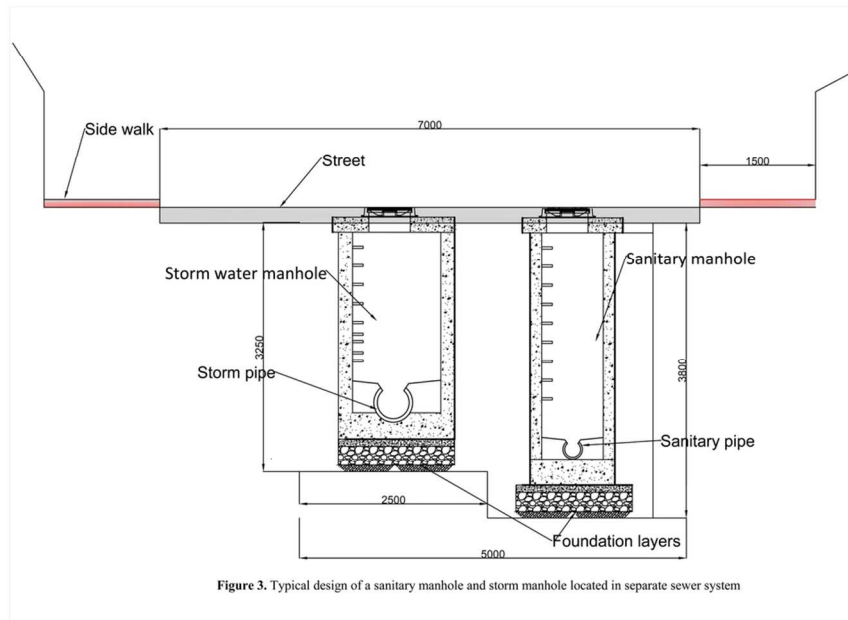


Fig. 3. Typical design of a sanitary manhole and storm manhole located in a separate sewer system

!! + !! + !! +

209x148mm (150 x 150 DPI)

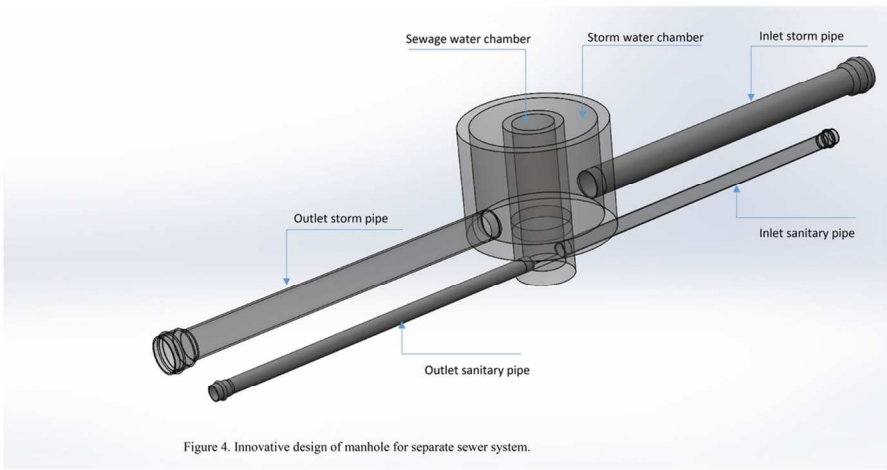


Fig 4. Innovative design of a manhole for separate sewer systems.
209x148mm (150 x 150 DPI)

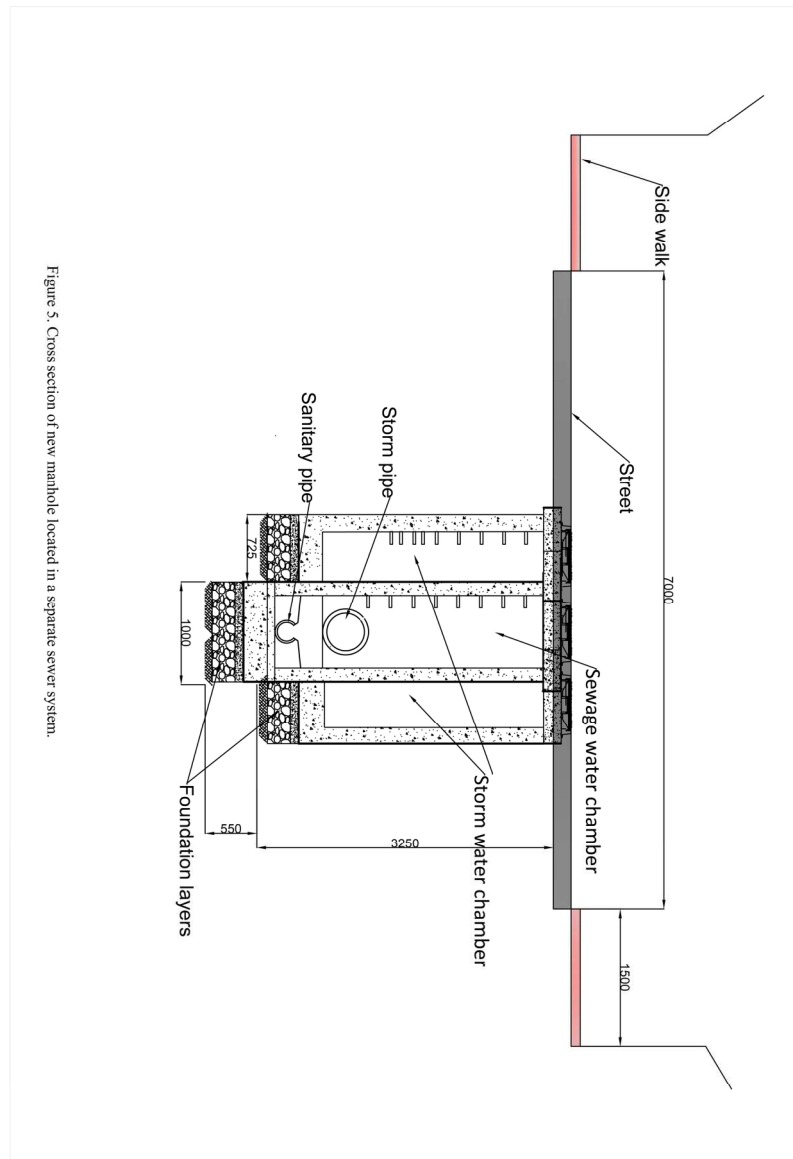


Figure 5. Cross section of new manhole located in a separate sewer system.

Fig. 5. Cross section of new manhole located in a separate sewer system.

297x420mm (150 x 150 DPI)



Fig. 6 a. Setup of the trench in the rig and location of measurement instruments on the new manhole surface at three points on the edge.



Fig. 6 b. Setup of the trench in the rig and location of measurement instruments on the new manhole surface at three points on the edge.

Fig. 6 a and b. Setup of the trench in the rig and location of measurement instruments on the new manhole surface at three points on the edge.

179x110mm (150 x 150 DPI)

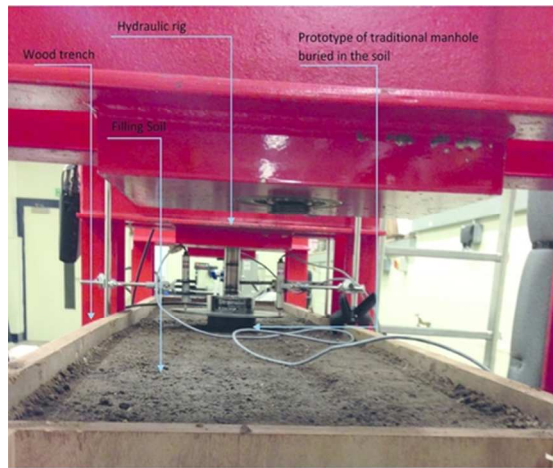


Fig. 7 a. Setup of the trench in the rig and location of measurement instruments on the traditional manhole surface at three points on the edge.



Fig. 7 b. Setup of the trench in the rig and location of measurement instruments on the traditional manhole surface at three points on the edge.

Fig. 7 a and b. Setup of the trench in the rig and location of measurement instruments on the traditional manhole surface at three points on the edge.

138x72mm (150 x 150 DPI)

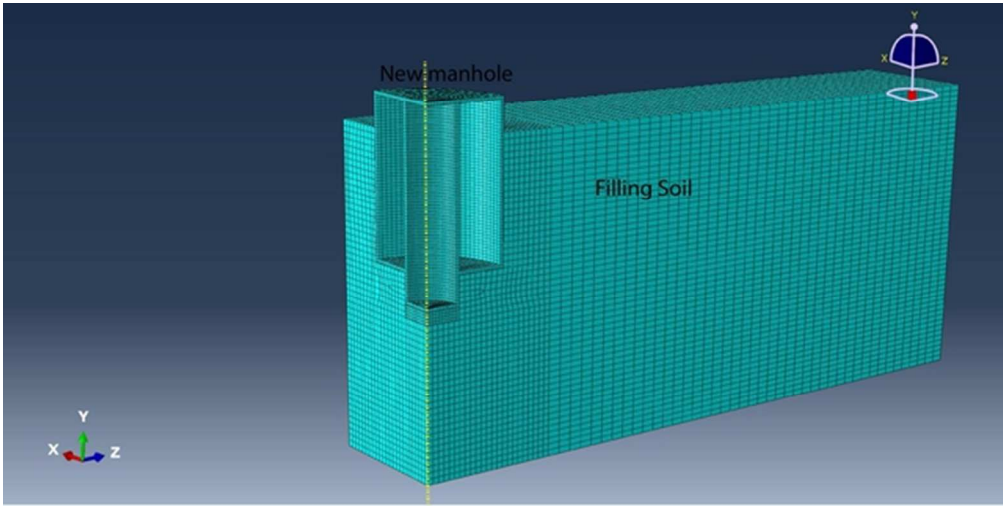


Figure 8. The symmetrical quarter of the new manhole FE mesh model represented the fully 3 D Manhole

Fig. 8. The symmetrical quarter of the new manhole FE mesh model representing the full 3D manhole
108x63mm (150 x 150 DPI)

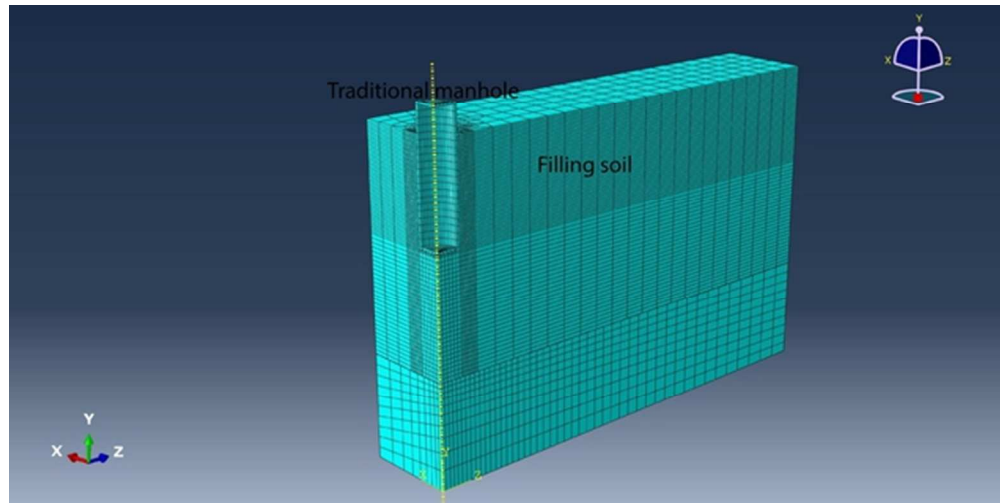


Figure 9. The symmetrical quarter of the traditional manhole FE mesh model represented the fully 3 D Manhole

Fig. 9. The symmetrical quarter of the traditional manhole FE mesh model representing the full 3D manhole

107x63mm (150 x 150 DPI)

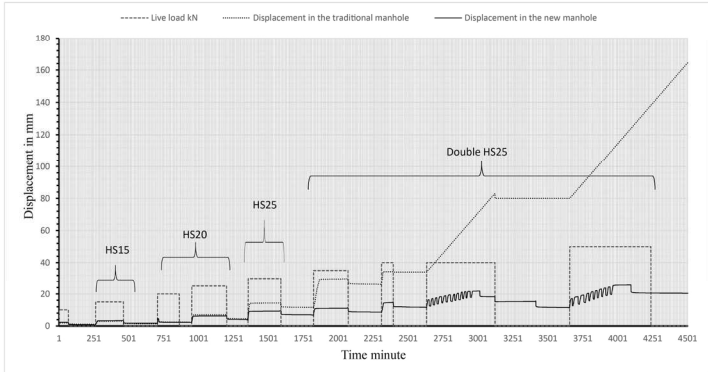


Fig. 10. Comparison between the new and traditional manholes under the same conditions and live loads.

Fig. 10. Comparison between the new and traditional manholes under the same conditions and live loads.

297x420mm (150 x 150 DPI)

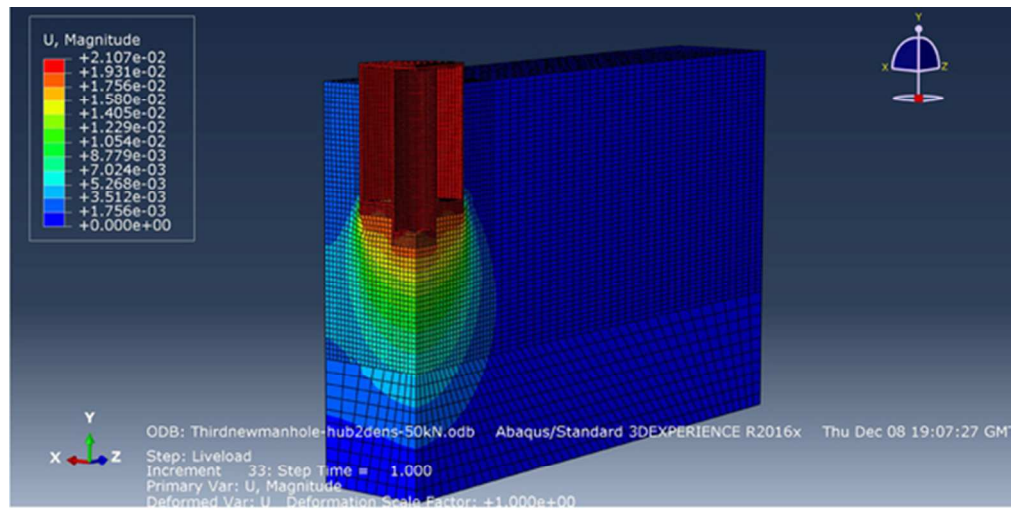


Fig. 11. The displacement of the new manhole at a double heavy load shown in a 3D quarter symmetric FEA model.

Fig. 11. The displacement of the new manhole at a double heavy load shown in a 3D quarter symmetric FEA model.

101x55mm (150 x 150 DPI)

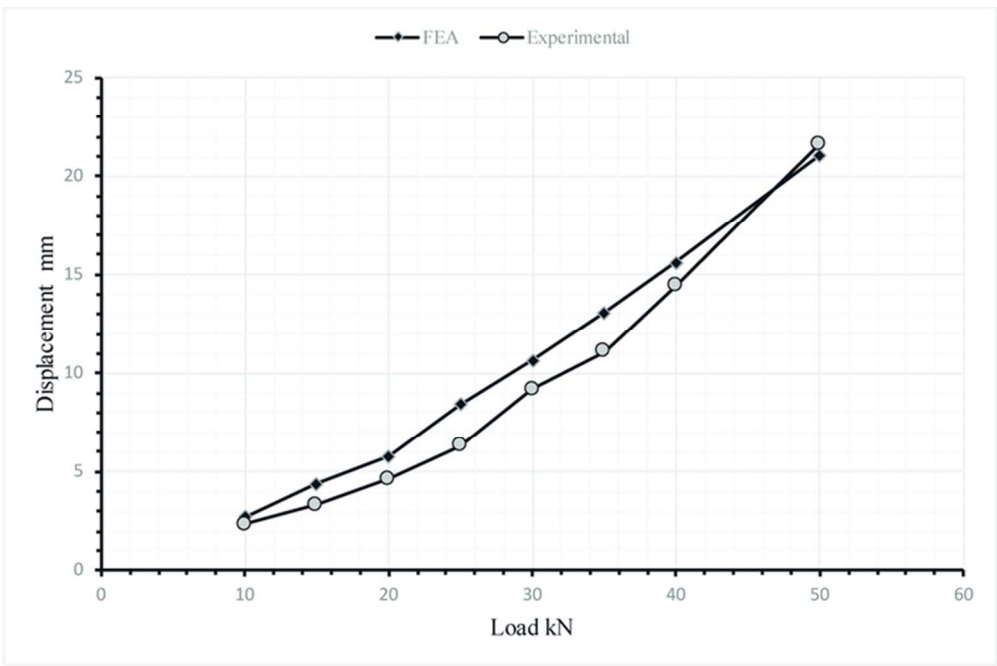


Fig. 12. Comparison of the displacements from both the experimental work and the FE model for the new manhole, in soil, under live loads.

Fig 12. Comparison of the displacements from both the experimental work and the FE model for the new manhole, in soil, under live loads.

128x96mm (150 x 150 DPI)

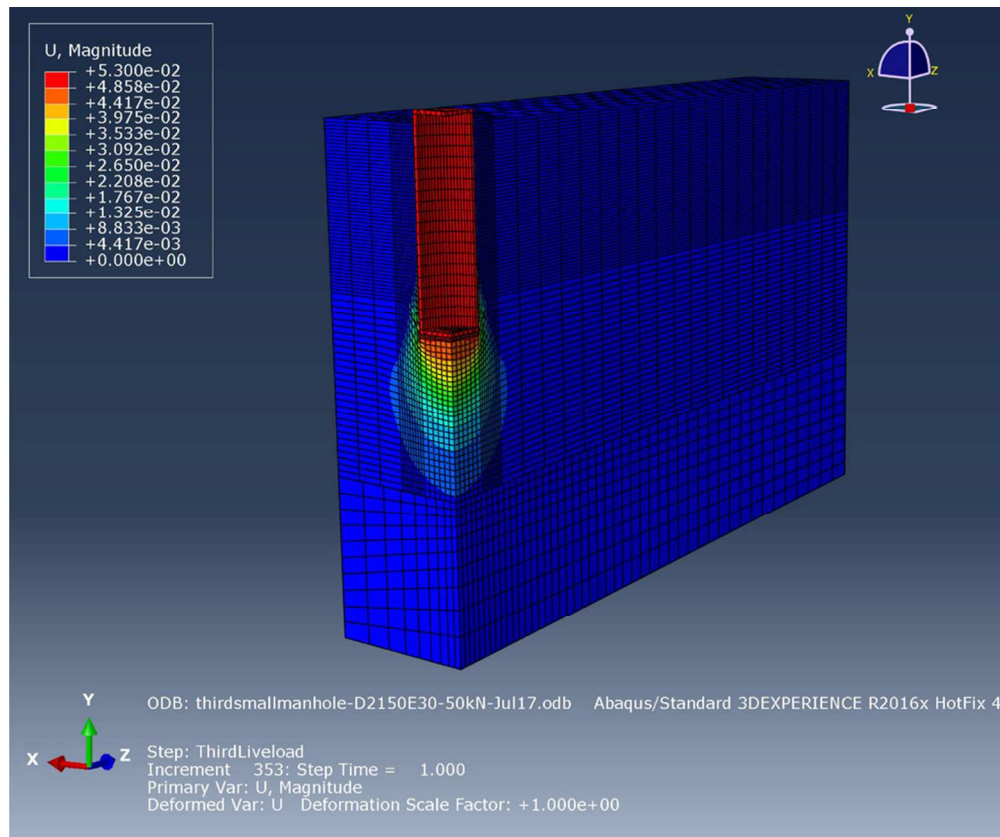


Fig. 13. The displacement of the traditional manhole at a double heavy load shown in a 3D quarter symmetric FEA model.

Fig. 13. The displacement of the traditional manhole at a double heavy load shown in a 3D quarter symmetric FEA model.

167x152mm (150 x 150 DPI)

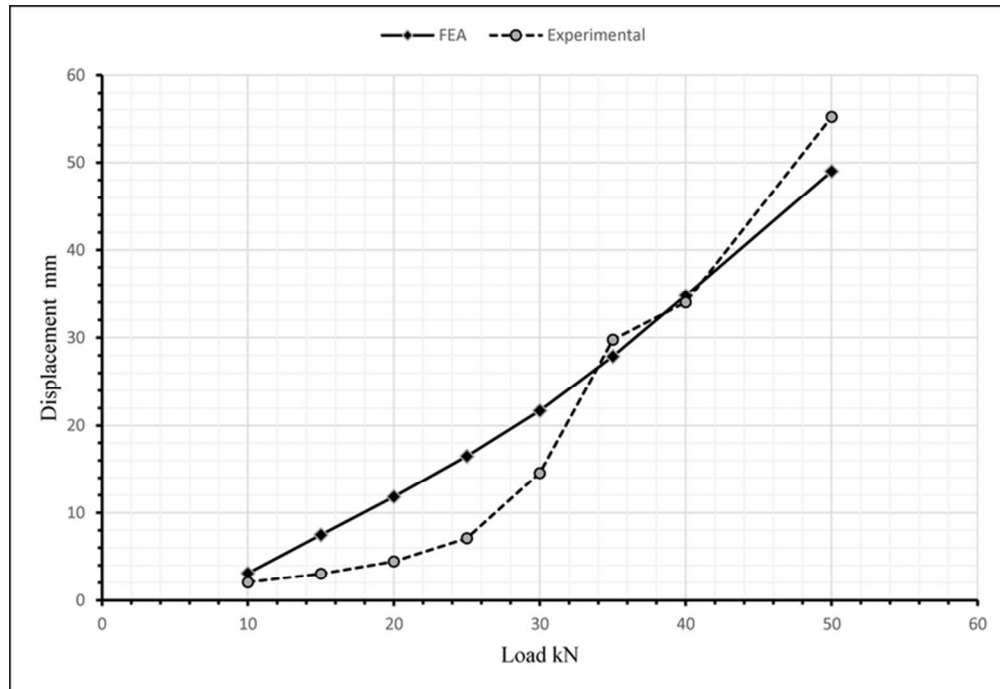


Fig. 14. Comparison of the displacement results from both experimental works and the FE model for the traditional manhole prototype in soil under live loads.

Fig. 14. Comparison of the displacement results from both experimental works and the FE model for the traditional manhole prototype in soil under live loads.

132x100mm (150 x 150 DPI)

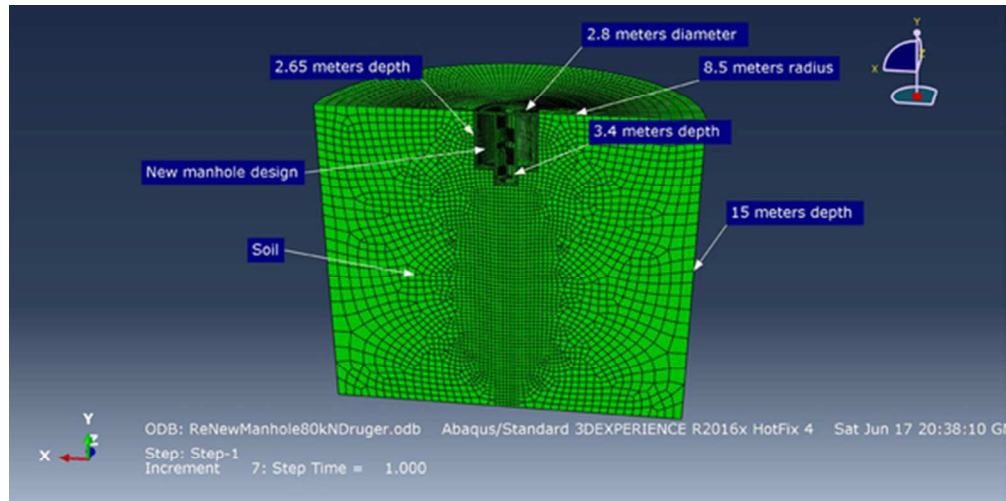


Fig. 15. Setup of the real scale of new manhole – soil model.

Fig 15. Setup of the real scale of new manhole – soil model.

100x54mm (150 x 150 DPI)

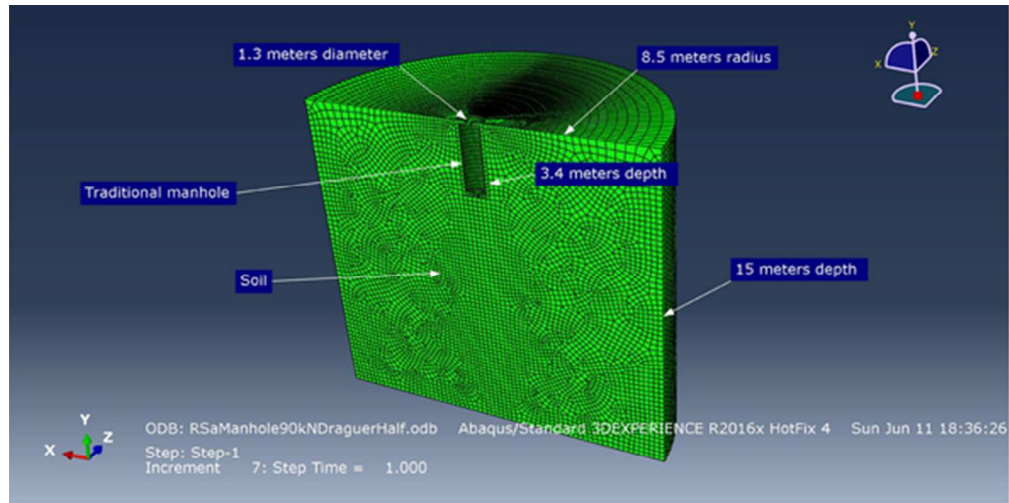


Fig. 16. Setup of the real scale of traditional manhole-soil model.

Fig. 16. Setup of the real scale of traditional manhole-soil model.

99x54mm (150 x 150 DPI)

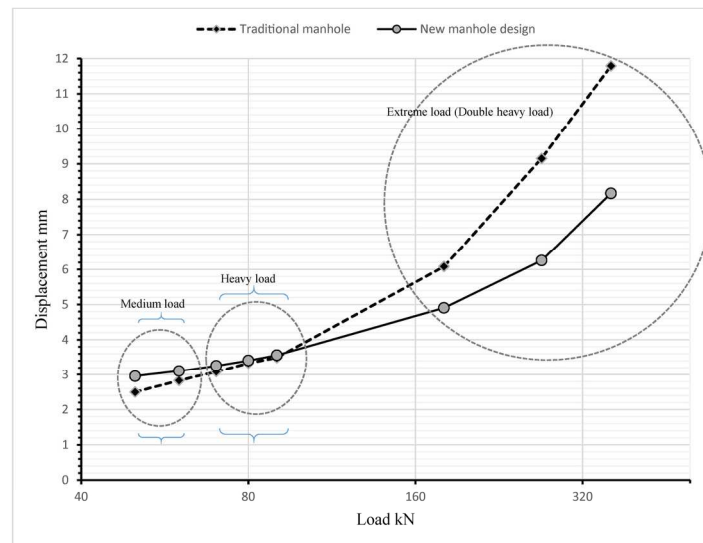


Fig. 17. A comparison of the displacement for both manholes under different loads (FE model).

Fig. 17. A comparison of the displacement for both manholes under different loads (FE model).

297x420mm (150 x 150 DPI)

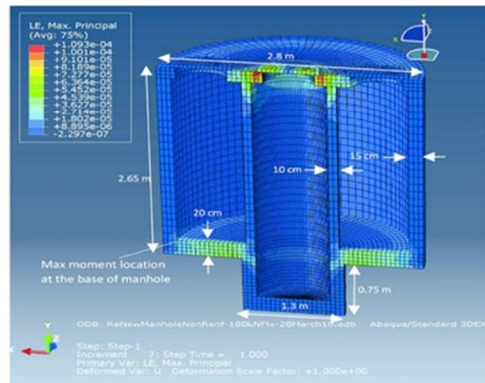


Fig. 18 a. The strains and location of maximum bending moment in the base of the new manhole body under a double heavy load (180kN).

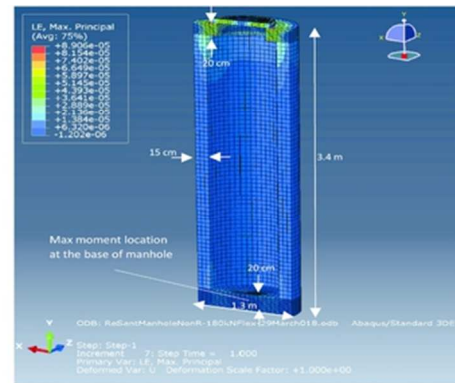


Fig. 18 b. The strains and location of maximum bending moment in the base of the traditional manhole body under a double heavy load (180kN).

Fig. 18 a. The strains and location of maximum bending moment in the base of the new manhole body under a double heavy load (180kN).
 Fig. 18 b. The strains and location of maximum bending moment in the base of the traditional manhole body under a double heavy load (180kN).

126x53mm (150 x 150 DPI)